INTEGRATING VEGETATION PHENOLOGY IN SOIL MOISTURE CHANGE DETECTION FROM ASAR WIDE SWATH IMAGES

Jasper Van doninck[1], Bernard De Baets[2], and Niko E.C. Verhoest[1]

[1]*Ghent University, Laboratory of Hydrology and Water Management, Coupure links 653, Ghent, Belgium, Email: Niko.Verhoest@UGent.be*

[2]*Ghent University, Department of Mathematical Modelling, Statistics and Bioinformatics, Coupure links 653, Ghent, Belgium*

ABSTRACT

Multitemporal processing of synthetic aperture radar imagery, e.g. for the extraction of a soil moisture index, requires normalization of acquisitions from different locations in space to a common incidence angle. Incidence angle dependence of backscatter is known to depend on the amount of aboveground vegetation, and can thus be expected to vary seasonally as a result of vegetation phenology. This study tries to assess the impact of vegetation phenology on the angular dependence, and the effect on a soil moisture index derived using a change detection method. It is found that soil moisture accuracy overall decreases when seasonality in the angular dependence of backscatter is ignored.

Key words: SAR; angular normalization; soil moisture; seasonality.

1. INTRODUCTION

The 10-year archive of imagery collected by the Advanced Synthetic Aperture Radar (ASAR) onboard ESA's ENVISAT platform offers opportunities for the derivation of spatially distributed soil moisture through multitemporal approaches. These approaches, where relative changes in backscatter are related to relative changes in soil moisture, are today already used in the operational soil moisture products for ERS's scatterometers and MetOp's advanced scatterometer (ASCAT) [15, 2, 7]. Data collected by the first Sentinel satellite will likely, in the near future, allow the production of high resolution soil moisture products.

Several multitemporal soil moisture retrieval methods were applied on synthetic aperture radar (SAR) data in the past. Shoshany et al. [10], for example, suggested to use a normalized difference of SAR backscatter of two images as an indicator of soil moisture changes between the times of image acquisition. On a larger time series of 10 SAR images over one month time, Wickel et al. [17] found strong correlations between soil moisture change and backscatter change for wheat stubble fields. Pathe et al. [8] presented a methodology, based on the scatterometer and ASCAT soil moisture retrieval algorithm, to derive a 1 km soil moisture index from ENVISAT ASAR in Global Monitoring (GM) mode and applied it to 697 ASAR GM images over Oklahoma. The same product was validated using in situ and airborne soil moisture data over an area in southeastern Australia [6].

SAR backscatter is, in addition to land surface properties (including vegetation cover, surface roughness and soil moisture content) and sensor properties (including signal frequency and polarization), also influenced by geometric properties [12]. Specifically, SAR backscatter depends on the angle of the incident radar signal, which is determined by the position of the sensor in space, the geographic location of the area under investigation and the local orientation of the terrain. When processing SAR data multitemporally, a normalization has to be performed to compensate for the effects of different incidence angles. Only under specific conditions, i.e. when different images are acquired from the same sensor's position in space, multitemporal data can be processed without prior normalization [e.g. 16].

Angular normalization techniques range from purely theoretical, e.g. based on Lambert's law for optics [12, 1], to purely empirical. Although more advanced techniques have been developed, many empirical normalization techniques consist of fitting a first [4, 8, 13] or second [17, 3, 5] order polynomial to a large number of incidence angle-backscatter coefficient couples. The polynomial coefficient(s) obtained from this fit can subsequently be used to normalize SAR backscatter coefficients to a common incidence angle.

The incidence angle dependence of radar backscatter is known to be influenced by, amongst others, the amount of aboveground vegetation, with the backscatter of bare soil varying strongly with incidence angle and backscatter over densely vegetated terrain exhibiting a more modest dependence [15]. Over vegetated surfaces, the angular dependence can thus be expected to vary throughout the year as a result of vegetation phenology or agricultural

practices. This seasonality has to be incorporated in the angular normalization in order to avoid the introduction of errors. For the coarse resolution real aperture radar systems ERS Scatterometer and MetOp ASCAT, the seasonal variation of the angular dependence of backscatter can be derived thanks to the multi-angular capabilities of these sensors and their short revisit time [15, 14, 7]. SAR systems, however, in general do not allow for multi-angular observations of a single location at a single moment in time. Polynomial angular normalization techniques therefore usually apply a single set of coefficients for the entire year. A number of studies [4, 3, 13], however, derived the angular dependence for a high vegetation season and a low vegetation season separately, resulting in significant differences between the two estimates.

This study analyses the seasonal variability on the angular dependence of backscatter, and the influence of this variability on the accuracy of soil moisture retrieval using a multitemporal time series of ENVISAT ASAR images.

2. STUDY AREA AND DATASETS

The peninsula of Calabria (Fig. 1) is situated in the southwestern tip of mainland Italy, measuring approximately 250 km in length and 30 km to 100 km in width, and is dissected longitudinally by a mountain range with elevations up to approximately 2000 m. Soil structure varies greatly, with clayey soils at the eastern side of the peninsula and more sandy soils at the western part.

Agriculture is concentrated in the lower elevation ranges and consists of both arable land and permanent crops. Of the latter, citrus and olive groves occur over large areas. Due to the Mediterranean climate, agriculture at the lower elevations is rainfall limited and (mainly cereal) crops exhibit a winter growing season. At the central plateaus, different growing cycles may occur as a result of lower temperatures and hence energy limited vegetation growth.

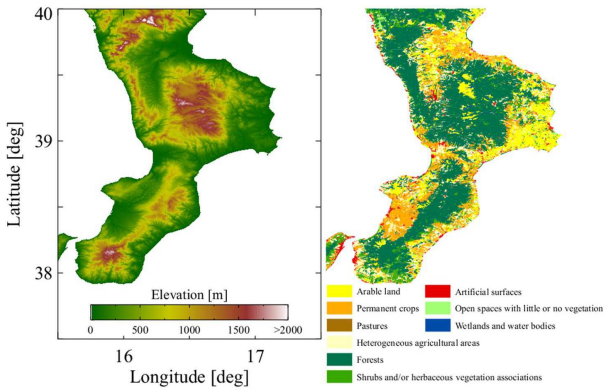

Figure 1. Left: topography of the study site. Right: Corine land cover 2000 map of the study site.

A total of 130 (87 descending and 43 ascending mode) Advanced Synthetic Aperture Radar Wide Swath (WS) images, completely or partially covering Calabria, were acquired between January 2008 and August 2011. The WS mode is one of the ScanSAR modes of ASAR and covers a swath of 405 km width with a spatial resolution of 150 m and a radiometric accuracy of approximately 0.6 dB. The temporal resolution is limited due to conflicting data acquisitions in other modes (especially over Europe) and the maximum duty cycle of 30 % in WS mode.

In order to validate the ASAR-derived soil moisture, a spatially distributed soil moisture model, inspired by the hydrological BEACH model of Sheikh et al. [9], was used. Details of this model, as well as its validation using in situ soil moisture measurements, are given in Van doninck et al. [13].

3. LINEARITY OF INCIDENCE ANGLE-BACKSCATTER RELATIONSHIP

ASAR WS images were topographically corrected (including masking of regions affected by radar shadow and/or layover) and radiometrically calibrated using the 10 m resolution digital elevation model TINITALY/01 that is available for the Italian territory [11] and resampled to a grid of 0.0025 ° (approximately 300 m) resolution. The preprocessing resulted for each ASAR WS pixel, for each acquisition date, in an incidence angle θ, expressed in degrees, and a corresponding backscatter coefficient $\sigma^0(\theta)$, expressed in dB.

Following Loew et al. [4], Pathe et al. [8], the dependence of $\sigma^0(\theta)$ on θ can be assessed assuming a linear relationship for the range of incidence angles covered by ASAR in WS mode (approximately 20 ° to 40 °):

$$\sigma^0(\theta) = \alpha + \beta\theta \,, \qquad (1)$$

where the polynomial coefficients α (in dB) and β (in dB/deg) are obtained for each pixel by fitting this relation to a large number of multitemporal (θ,$\sigma^0(\theta)$) couples. The coefficient β can subsequently be used to normalize ASAR backscatter at incidence angle θ to a common incidence angle.

The rationale behind the use of this linear relationship is that, although the relation between incidence angle and backscatter is typically not linear [12], it can be considered as such for the limited incidence angle range in which the ASAR instrument operates. When using both ascending and descending mode images, however, the incidence angle range will extend beyond the typical range of 20 °– 40 ° for pixels over sloped terrain. For a slope of 20 °, for example, the incidence angle range can increase to 0 °– 60 °, a range for which the linear approximation of the angular dependence is not necessarily valid. Fig. 2 shows examples of the θ–$\sigma^0(\theta)$ relationship for two pixels, one over relatively flat terrain and one over strongly sloped terrain. While the small range of θ over modest topography results in a relationship that can be approximated as linear, it is clear that the large range over sloped

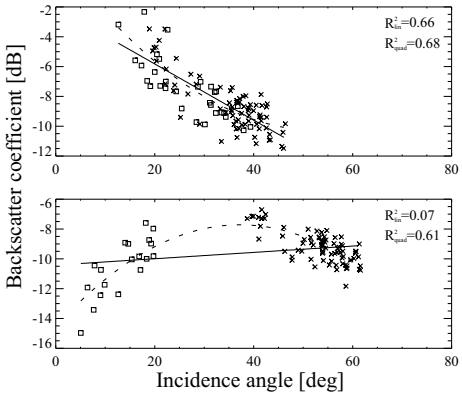

Figure 2. Scatterplot of backscatter coefficient versus incidence angle for ascending mode (boxes) and descending mode (crosses) images over two example pixels, together with coefficients of determination of linear fit (R^2_{lin}, full line) and second order polynomial fit (R^2_{quad}, dashed line).

terrain can result in severe non-linearity. When considering ascending and descending mode images separately, however, the θ–$\sigma^0(\theta)$ relationship can be approximated by a linear function irrespective the terrain slope. Therefore, only descending mode images will be used in the remainder of this study. Ascending mode images could be processed separately in a similar way.

4. SEASONALITY IN ANGULAR DEPENDENCE OF BACKSCATTER

The first order polynomial coefficient or angular correction coefficient can, for each pixel of the study site, be obtained by fitting Equation 1 to all available (θ,$\sigma^0(\theta)$) couples. The thus derived β_{year} is given in Fig. 3(a). It is observed that more negative values correspond to more sparsely vegetated terrain such as arable land, while values close to zero occur over forests.

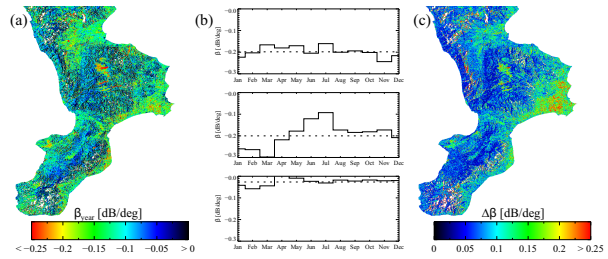

Figure 3. Value of the polynomial coefficient β_{year} for each pixel in the study site (a). Temporal behaviour of β_{month} (full line), as well as β_{year} (dotted line) for three example pixels over (top to bottom) permanent crops, arable land and deciduous forest (b). Difference between maximum and minimum value of β_{month} for each pixel in the study site (c).

Instead of deriving α and β in Equation 1 using the entire multitemporal dataset, they can also be produced for each month of the year individually by only using (θ,$\sigma^0(\theta)$) couples from that specific month, thus incorporating the effects of vegetation phenology. Here, the polynomial coefficients are derived on a monthly basis, fitting Eq. 1 to the (θ,$\sigma^0(\theta)$) couples of a sliding 3-month window over all the years, i.e. β_{month} for the month of January is derived using observations during December, January and February from 2008 to 2011. For larger datasets, the size of this temporal window could be reduced in order to increase the temporal resolution of the slope estimates. Fig. 3(b) shows the temporal behaviour of β_{month} for three examples pixels over permanent crops, arable land and deciduous forest, as well as β_{year} for these pixels. It is observed that β for the arable land pixel shows much more seasonal variability than the other land cover types. This is confirmed when considering the difference between maximum and minimum values of β_{month} ($\Delta\beta$) given in Fig. 3(c). $\Delta\beta$ is found to be in the order of magnitude of β_{year}.

Incidence angles are normalized as:

$$\sigma^0(\theta_{\mathrm{ref}}) = \sigma^0(\theta) - \beta(\theta - \theta_{\mathrm{ref}})\,, \qquad (2)$$

where the reference incidence angle θ_{ref} is defined for each pixel individually as the average of the minimum and maximum value of θ for that pixel. Two normalizations are performed, one by replacing β in Eq. 2 by β_{year}, the other using β_{month}. The influence of using different values of β is assessed in the following section.

5. ACCURACY OF SOIL MOISTURE RETRIEVAL

In a last step, a relative soil moisture index for each pixel of the study site is derived for each available descending mode ASAR WS image. The change detection approach as applied by, e.g., Pathe et al. [8] is applied here:

$$\mathrm{SMI} = \frac{\sigma^0(\theta_{\mathrm{ref}}) - \sigma^0_{\mathrm{dry}}}{S}\,, \qquad (3)$$

where SMI is a relative soil moisture index, σ^0_{dry} is the dry reference backscatter, defined as the lowest value of $\sigma^0(\theta_{\mathrm{ref}})$ in the time series, and S is the sensitivity, defined as the difference between the highest and lowest value of $\sigma^0(\theta_{\mathrm{ref}})$ in the time series.

The ASAR-derived soil moisture is validated for each pixel through the coefficient of correlation (R) between ASAR soil moisture and modelled soil moisture (Fig. 4(a)). It is observed that soil moisture can be predicted relatively accurate over most arable land areas, and that moderate to low values of R occur over permanent crops and forests.

The values given in Fig. 4(a) refer to the soil moisture index obtained from $\sigma^0(\theta_{\mathrm{ref}})$ values derived using β_{month}. When deriving the soil moisture index using the yearly

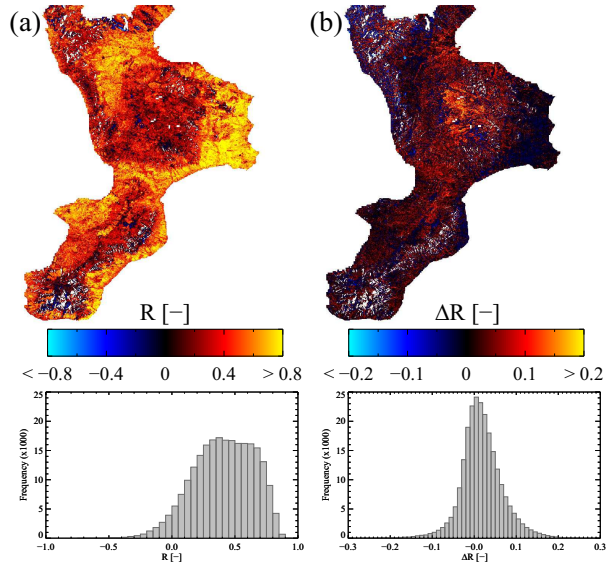

Figure 4. Validation of the soil moisture index (in terms of correlation coefficient) obtained after normalizing ASAR WS backscatter using β_{month} (a). Decrease in correlation coefficient when replacing β_{month} by β_{year} (b).

correction coefficient β_{year}, correlation coefficients on average decrease. Decrease in R is given in Fig. 4(b). Regions with the strongest decreases in R do, however, not correspond to the regions with the largest variability of the angular correction coefficient. This is because the error on the soil moisture estimate is strongly influenced by the sensitivity of radar backscatter, or the difference in backscatter over wet and dry conditions, with larger sensitivity resulting in a smaller error [8]. In this study, regions of high seasonality in β_{month} correspond to regions with large sensitivities.

6. CONCLUSION

This study investigated the influence of vegetation phenology on the angular dependence of ASAR WS backscatter and on a soil moisture index derived through a change detection method. In a first step, it was investigated whether the assumption of a linear relationship between incidence angle and backscatter was valid for the study site, the peninsula of Calabria, Italy. It was shown that strong topography in the study site can result in a strong non-seasonality of this relationship, when both ascending and descending mode images are considered. When using only data obtained in one mode, however, the relationship can be approximated as linear. In a second step, it was shown that the angular dependence of ASAR backscatter can vary considerably throughout the year, depending on landcover. Crops on arable land in particular are responsible for large differences in angular dependence. Finally, the accuracy of a soil moisture retrieval method was assessed using a hydrological model based on meteorological data and a soil map. It was shown that spatial changes in soil moisture can be detected using ASAR WS images when vegetation cover is relatively low. Over forests, retrieval accuracies are low. When neglecting seasonality in the angular dependence of backscatter, soil moisture retrieval accuracies on average decrease.

ACKNOWLEDGEMENTS

ASAR WS images were provided by the European Space Agency under the Category-1 Proposal 6944.

REFERENCES

[1] Abdel-Messeh, M. and Quegan, S. (2000). Variability in ERS Scatterometer measurements over land. *IEEE Transactions on Geoscience and Remote Sensing*, 38(4), 1767–1776.

[2] Bartalis, Z., Wagner, W., Naeimi, V., Hasenauer, S., Scipal, K., Bonekamp, H., Figa, J., and Anderson, C. (2007). Initial soil moisture retrieval from the METOP-A Advanced Scatterometer (ASCAT). *Geophysical Research Letters*, 34(20), L20401.

[3] Baup, F., Mougin, E., de Rosnay, P., Timouk, F., and Chênerie, I. (2007). Surface soil moisture estimation over the AMMA Sahelian site in Mali using ENVISAT/ASAR data. *Remote Sensing of Environment*, 109, 473–481.

[4] Loew, A., Ludwig, R., and Mauser, W. (2006). Derivation of surface soil moisture from ENVISAT ASAR wide swath and image mode data in agricultural areas. *IEEE Transactions on Geoscience and Remote Sensing*, 44(4), 889–899.

[5] Mladenova, I. and Lakshmi, V. (2009). Terrain: slope influence on QuikSCAT backscatter. *IEEE Transactions on Geoscience and Remote Sensing*, 47(8), 2722–2732.

[6] Mladenova, I., Lakshmi, V., Walker, J. P., Panciera, R., Wagner, W., and Doubkova, M. (2010). Validation of the ASAR Global Monitoring Mode soil moisture product using the NAFE'05 data set. *IEEE Transactions on Geoscience and Remote Sensing*, 48(6), 2498–2508.

[7] Naeimi, V., Scipal, K., Bartalis, Z., Hasenauer, S., and Wagner, W. (2009). An improved soil moisture retrieval algorithm for ERS and METOP scatterometer observations. *IEEE Transactions on Geoscience and Remote Sensing*, 47(7), 1999–2013.

[8] Pathe, C., Wagner, W., Sabel, D., Doubkova, M., and Basara, J. B. (2009). Using ENVISAT ASAR Global Mode data for surface soil moisture retrieval over Oklahoma, USA. *IEEE Transactions on Geoscience and Remote Sensing*, 47(2), 468–480.

[9] Sheikh, V., Visser, S., and Stroosnijder, L. (2009). A simple model to predict soil moisture: Bridging

event and continuous hydrological (BEACH) modelling. *Environmental Modelling & Software*, 24, 542–556.

[10] Shoshany, M., Svoray, T., Curran, P. J., Foody, G. M., and Perevolotsky, A. (2000). The relationship between ERS-2 SAR backscatter and soil moisture; generalization from a humid to semi-arid transect. *International Journal of Remote Sensing*, 21(11), 2337–2343.

[11] Tarquini, S., Vinci, S., Favalli, M., Doumaz, F., Fornaciai, A., and Nannipieri, L. (2012). Release of a 10-m-resolution DEM for the Italian territory: Comparison with global-coverage DEMs and anaglyph-mode exploration via the web. *Computers & Geosciences*, 38, 168–170.

[12] Ulaby, F. T., Moore, R. K., and Fung, A. K. (1982). *Microwave Remote Sensing: Active and Passive, volume II: Radar Remote Sensing and Surface Scattering and Emission Theory*. Artech House, Boston.

[13] Van doninck, J., Peters, J., Lievens, H., De Baets, B., and Verhoest, N. E. C. (2012). Accounting for seasonality in a soil moisture change detection algorithm for ASAR Wide Swath time series. *Hydrology and Earth System Sciences*, 16, 773–786.

[14] Wagner, W., Lemoine, G., Borgeaud, M., and Rott, H. (1999a). A study of vegetation cover effects on ERS Scatterometer data. *IEEE Transactions on Geoscience and Remote Sensing*, 37(2), 938–948.

[15] Wagner, W., Noll, J., Borgeaud, M., and Rott, H. (1999b). Monitoring soil moisture over the Canadian Prairies with the ERS Scatterometer. *IEEE Transactions on Geoscience and Remote Sensing*, 37(1), 206–216.

[16] Wall, J., Collingwood, A., and Treitz, P. (2010). Monitoring surface moisture state in the Canadian High Arctic using synthetic aperture radar (SAR). *Canadian Journal of Remote Sensing*, 36(S1), S124–S134.

[17] Wickel, A. J., Jackson, T. J., and Wood, E. F. (2001). Multitemporal monitoring of soil moisture with RADARSAT SAR during the 1997 Southern Great Plains hydrology experiment. *International Journal of Remote Sensing*, 22(8), 1571–1583.